Giant Shapiro Steps with Screening Currents

D. Domínguez[a] and Jorge V. José

Physics Department, Northeastern University, Boston, Massachusetts 02115

(Received 13 April 1992)

We present a detailed study of the dynamic response of overdamped Josephson-junction square arrays driven by a dc plus ac current, including self-induced magnetic-field effects, as a function of a parameter κ. The transition from type-II ($\kappa > 1$) to type-I ($\kappa < 1$) behavior is studied in detail. It is found that the IV characteristics show fractional giant Shapiro steps, with and without external magnetic fields, with microscopic coherent vortex dynamics fundamentally different in the two extreme κ limits. Our results in zero external magnetic field are in good agreement with recent experiments in Nb-Au-Nb arrays.

PACS numbers: 74.50.+r, 74.60.Jg, 85.25.Dq

The recent discovery [1] of fractional giant Shapiro steps (FGSS) in dc plus ac current driven Josephson-junction arrays (CDJJA), in the presence of a transverse magnetic field with frustration $f=\Phi/\Phi_0=p/q$, where Φ is the magnetic flux through a plaquette, Φ_0 is the quantum of flux, and (p,q) are relative primes, has motivated several interesting experimental [2,3] and theoretical [4,5] studies. The FGSS were found in proximity-effect CDJJA and appear as plateaus in the time-averaged voltage $V_q=N(n/q)\hbar\omega/2e$, with n an integer, $\omega=2\pi\nu$ the ac current frequency, and N the number of junctions along the current direction. These results have been explained through studies of an overdamped resistively shunted junction (RSJ) model, in terms of a collective motion of the ground-state vortex lattice configurations induced by the $f=p/q$ external field [4]. Giant half-integer steps in the IV characteristics have been identified with a different type of axisymmetric coherent vortex state (ACVS) present in the case where there is no external magnetic field [6].

The experiments have been carried out for the most part in proximity-effect arrays that have strong temperature-dependent critical currents [1–3]. A carefully controlled narrow temperature range was studied [1] in order to minimize the self-induced magnetic-field (SIMF) effects in the experiments. Previous theoretical studies of FGSS have not included these effects. However, other authors have shown experimentally that SIMF effects can be essential for understanding their data [3]. This paper presents a detailed analysis of the dynamic response of a CDJJA including the SIMF effects. We analyze the continuous transition from type-II ($\kappa > 1$) to type-I ($\kappa < 1$) behavior, as a function of $\kappa \equiv \lambda_L/a$, with λ_L a London screening length, defined below in terms of the self and nearest-neighbor mutual inductances of the current loops in the array, and a the lattice spacing, which plays the role of a coherence length. For all the κ values considered, we find a series of fractional giant plateaus in the IV characteristics, even when there are no external magnetic fields applied. It is important that for $\kappa < 1$ the giant Shapiro steps are not found to be due to coherent oscillations of ground-state vortex configurations, as is the case in the $\kappa \gg 1$ limit with $f=p/q\neq 0$.

The model studied in this paper is defined by the "coarse-grained action"

$$\mathcal{F} = -\sum_{\hat{\mu},\mathbf{r}} E_J \cos[\Delta_{\hat{\mu}}\theta(\mathbf{r},t) - A_{\hat{\mu}}(\mathbf{r},t)] - \sum_{\mathbf{r},\mu_y} I^e(t)[\Delta_{\mu_y}\theta(\mathbf{r},t) - A_{\mu_y}(\mathbf{r},t)] + \tfrac{1}{2}\sum_{\mathbf{R},\mathbf{R}'} [\Phi(\mathbf{R},t)-\Phi^e(\mathbf{R})]\Lambda^{-1}(\mathbf{R},\mathbf{R}')[\Phi(\mathbf{R}',t)-\Phi^e(\mathbf{R}')] . \quad (1)$$

The variables included in the definition of $\mathcal{F}$ are the following: The order-parameter phase difference between the two superconductors forming a Josephson junction is $\Delta_{\hat{\mu}}\theta(\mathbf{r},t)=\theta(\mathbf{r}+\hat{\mu},t)-\theta(\mathbf{r},t)$. Here $(\mathbf{r},\hat{\mu})$ labels the links in a square lattice with end points at the lattice sites $\mathbf{r}$ and $\mathbf{r}+\hat{\mu}$ with $\hat{\mu}$ a unit vector along the x or y axis. The total flux $\Phi(\mathbf{R},t)$ through a given plaquette centered at $\mathbf{R}$ is given by $\Phi(\mathbf{R},t)=\Phi^e(\mathbf{R})+\sum_{\mathbf{R}'}\Lambda(\mathbf{R},\mathbf{R}')J(\mathbf{R}',t)$, where $\Phi^e(\mathbf{R})$ is the flux due to the external field, $J(\mathbf{R},t)$ is the current flowing around the plaquette at $\mathbf{R}$, and $\Lambda(\mathbf{R},\mathbf{R}')$ is the mutual inductance matrix that determines how the screening currents modify the external field. A general expression for this matrix, as applied to a square array, is not known in detail. In this paper we consider a model of $\Lambda(\mathbf{R},\mathbf{R}')$ that only includes the self and nearest-neighbor mutual inductance contributions. The gauge link variable is $A_{\hat{\mu}}(\mathbf{r},t)=(2\pi/\Phi_0)\int_{\mathbf{r}}^{\mathbf{r}+\hat{\mu}}\mathbf{A}\cdot d\mathbf{l}$, with $\mathbf{A}$ the total vector potential and $2\pi\Phi(\mathbf{R},t)/\Phi_0 = \Delta_{\hat{\mu}}\wedge A_{\hat{\mu}}(\mathbf{r},t)$. The Josephson coupling constant is $E_J=(\Phi_0/2\pi)I_c$, with I_c the critical current which is taken to be the same for all junctions. The external current applied at the bottom of the array along the y direction enters as a boundary condition in Eq. (1) with $I^e(t) = I_{\rm dc}+I_{\rm ac}\sin(2\pi\nu t)$.

We are interested in studying the dynamics of $\theta(\mathbf{r},t)$

and $\Phi(\mathbf{R},t)$ self-consistently. The dynamical equations are taken to be given by the RSJ model for θ and Faraday's law for Φ. Each one of the two dynamical variables has its own characteristic frequency, $\nu_\theta = 2\pi\mathcal{R}I_c/\Phi_0$, and $\nu_\Phi = \mathcal{R}/\bar{\Lambda}$, where $\bar{\Lambda}$ is an effective inductance that depends on the specific model for $\Lambda(\mathbf{R},\mathbf{R}')$, and $\mathcal{R}$ is the shunt resistance along all the links in the lattice. In the linearized regime of the Josephson term in Eq. (1) we can identify $\kappa = (2\pi I_c\bar{\Lambda}/\Phi_0)^{1/2} = \lambda_L/a$, or in terms of the characteristic frequencies, $\kappa^2 = \nu_\Phi/\nu_\theta$. Taking this relation into account is essential to the implementation of an efficient numerical algorithm to study the problem. In the extreme type-II regime the fast variables are the fluxes while the θ's are slow, with the opposite happening in the extreme type-I regime. This situation is typical of "stiff" problems in ordinary differential equations, which are notoriously difficult to treat numerically and even analytically, for they lead to singular perturbations [7]. On the other hand, since the equations of motion are gauge invariant we can use this symmetry to find the most appropriate gauge to solve the problem. It turns out that one specific gauge does not allow us to efficiently solve the problem for all values of κ. In the $\kappa \gg 1$ limit, a convenient gauge to choose is the Coulomb gauge given by $\Delta_{\hat{\mu}} \cdot A_{\hat{\mu}} = 0$. We have implemented an algorithm that works in this case. Our discussion concentrates on the intermediate regime $0.1 \leq \kappa^2 \leq 10$, where the stiffness problem is less severe. As we shall see below this is an experimentally realizable regime. It is convenient to use the temporal gauge to efficiently solve the problem in this range of parameters. This gauge entails the replacement $\Delta_{\hat{\mu}}\theta(\mathbf{r},t) - A_{\hat{\mu}}(\mathbf{r},t) \rightarrow \Psi_{\hat{\mu}}(\mathbf{r},t)$. This gauge has been used extensively in the past [8] and more recently within the context of a JJA model of ceramic high-temperature superconductors [9]. In terms of $\Psi_{\hat{\mu}}$ the Langevin RSJ dynamical equations of motion are given by

$$\Gamma\frac{\partial}{\partial t}\Psi_\mu(\mathbf{r},t) = -\frac{\delta\mathcal{F}}{\delta\Psi_\mu(\mathbf{r},t)} + \eta_{\hat{\mu}}(r,t)\,. \tag{2}$$

The Langevin white-noise function $\eta_{\hat{\mu}}(r,t)$ has correlations

$$\langle \eta_{\hat{\mu}}(\mathbf{r},t)\eta_{\hat{\mu}'}(\mathbf{r}',t')\rangle = 2\Gamma k_B T\delta_{\mathbf{r},\mathbf{r}'}\delta_{\hat{\mu},\hat{\mu}'}\delta(t-t')\,,$$

where T is the temperature, k_B is Boltzmann's constant, and the dissipation parameter is $\Gamma = (\Phi_0/2\pi)^2\mathcal{R}^{-1}$. The flux at $\mathbf{R}$ is calculated from

$$2\pi\Phi(\mathbf{R},t)/\Phi_0 = -\Delta_{\hat{\mu}}\wedge\Psi_{\hat{\mu}} \equiv -\Psi_{\mu_x}(\mathbf{r}) + \Psi_{\mu_x}(\mathbf{r}+\mu_y) - \Psi_{\mu_y}(\mathbf{r}+\mu_x) + \Psi_{\mu_y}(\mathbf{r})\,.$$

Equation (2) represents a set of N^2 coupled nonlinear stochastic equations driven by the external current. To allow the internal and external magnetic fields to relax to their correct stationary values we have to take free end boundary conditions in the direction perpendicular to the current. This implies that relatively large lattices have to be simulated to get physically correct asymptotic behavior. We have developed an efficient numerical algorithm [10], in the spirit of those used in Refs. [5,6], that takes all these constraints into account.

We proceed to present the results from calculations using two models for the inductance matrix. In the presence of a nonzero f we find that it is sufficient to use the self-inductance model $\Lambda(\mathbf{R},\mathbf{R}') = \Lambda\delta_{\mathbf{R},\mathbf{R}'}$. On the other hand, in the zero-field case it is essential, as found experimentally [3(b)], to include the edge fields. We model the edge-field effects in terms of an inductance matrix defined as $\Lambda(\mathbf{R},\mathbf{R}') = \Lambda\delta_{\mathbf{R},\mathbf{R}'} - M\delta_{\mathbf{R},\mathbf{R}'\pm\hat{\mu}}$, with Λ and M constants. In this case $\bar{\Lambda} = \Lambda - 4M$, and the edge magnetic fields $B_{\text{edge}} \sim \pm MI^e/a^2$. Including the M term is equivalent to having a finite demagnetization factor d in the array, with d defined from $\Delta H = -d\mathcal{M}$ and $d = -\Lambda^{-1}\sum_{\mathbf{R}'\neq\mathbf{R}}\Lambda(\mathbf{R},\mathbf{R}')$, where ΔH is the difference between the external and internal magnetic fields. The total magnetization $\mathcal{M}$ is proportional to $\sum_{\mathbf{R}}J(\mathbf{R})$. In an external field the array behaves as having an effective self-inductance $\bar{\Lambda} = (1-d)\Lambda(\mathbf{R},\mathbf{R})$. In the diagonal case $d=0$, in the nearest-neighbor approximation $d = 4M/\Lambda$, and in the infinite sample limit $d \rightarrow 1$. From our results we believe that this approximation for $\Lambda(\mathbf{R},\mathbf{R}')$ qualitatively captures the essence of the self-field effects.

In Figs. 1(a) and 1(b) we show results for the IV characteristics of systems with 40×40 lattice sites with $f = \frac{1}{3}$ and $\Lambda(\mathbf{R},\mathbf{R}') = \Lambda\delta_{\mathbf{R},\mathbf{R}'}$. Figure 1(a) shows the results for $\kappa = 2.27$, while Fig. 1(b) has $\kappa = 0.44$. Note that the value of $\bar{\Lambda}$ is implicit in the value of κ in the type-II regime. In the type-I regime we choose to give the results as a function of κ and d instead of Λ and M, for these pa-

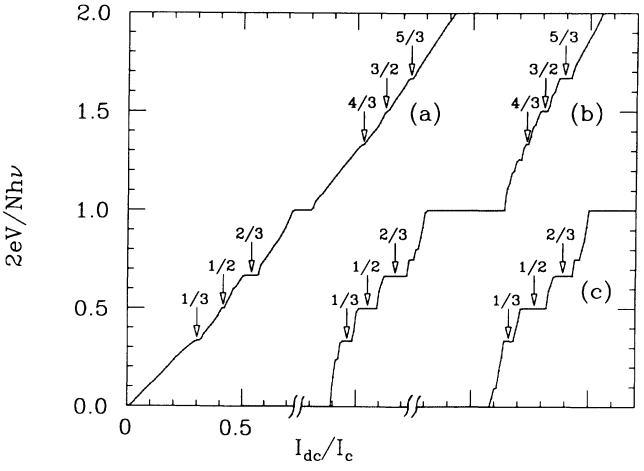

FIG. 1. IV characteristics for $f = \frac{1}{3}$, $I_{ac} = I_c$, $\nu = 0.1\nu_\theta$, $M = 0$, for lattice size 40×40. (a) Type-II array with $\kappa = 2.27$; (b) type-I array with $\kappa = 0.44$; (c) the same as (b) including edge fields with $M/\Lambda = 0.1$ ($d = 0.4$). The giant Shapiro steps at $n/3$ and $n/2$ are marked. Curves start about the same place and are displaced for clarity.

rameters permit a more direct comparison to experiment. It is clear from these results that in both limits the IV's show giant Shapiro steps at $\frac{1}{3}$ and $\frac{1}{2}$ fractions. We note that for $\kappa > 1$ there is a small $\frac{1}{2}$ step, as was found when $\kappa = \infty$ using free boundary conditions (Lee and Stroud [4]), while for $\kappa < 1$ the $\frac{1}{2}$ step is much bigger. There are also higher harmonics seen in the type-I IV curves that we have not highlighted in the figure for clarity. In Fig. 2(a) the widths of the $\frac{1}{3}$, $\frac{2}{3}$, and $\frac{1}{2}$ steps are plotted as a function of $1/\kappa$. For comparison, in Fig. 2(a) we show the results for the $\frac{1}{2}$-step width as a function of κ for $f = \frac{1}{2}$. We distinguish three qualitatively different κ regimes in this figure: (i) the type-II regime where the step width remains essentially constant and equal to the $\kappa = \infty$ result and the type-I regime where the step width (ii) *increases* initially and then (iii) decreases. The decrease occurs when the characteristic frequency $\nu_\Phi < \nu$,

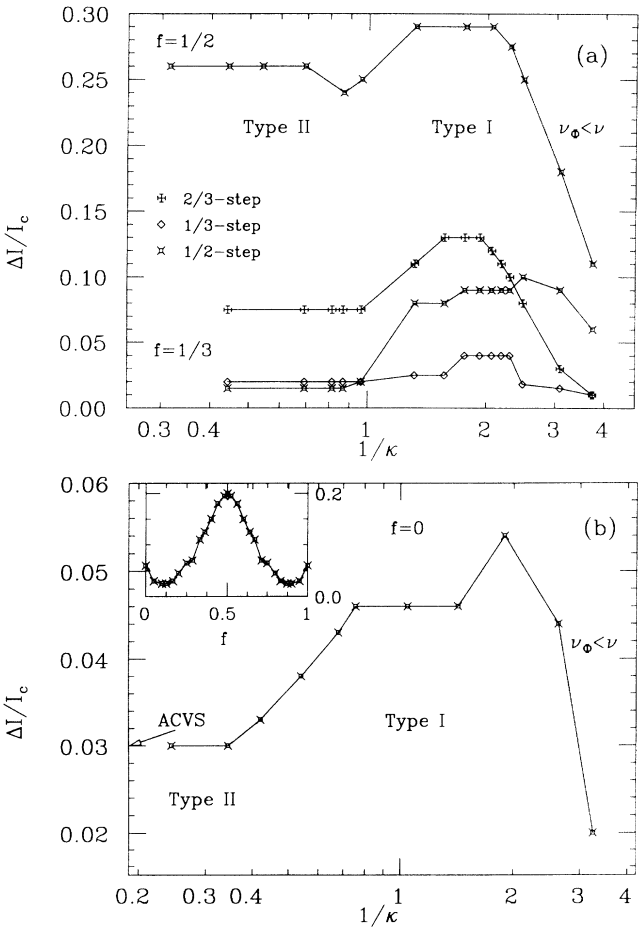

FIG. 2. IV step widths, $\Delta I/I_c$ vs $1/\kappa$, for $I_{ac} = I_c$, $\nu = 0.1\nu_\theta$, $M = 0$, and lattice size 40×40. (a) The upper curve corresponds to the $\frac{1}{2}$ step for $f = \frac{1}{2}$, while the three lower curves correspond to the $\frac{2}{3}$, $\frac{1}{3}$, and $\frac{1}{2}$ steps with $f = \frac{1}{3}$. (b) Same as (a) for the $\frac{1}{2}$ step in zero field and keeping constant $d = 0.4$. Inset: The width of the $\frac{1}{2}$ step as a function of f for $\kappa = 0.44$ and the same parameters as above.

which means that the current distributions are not able to follow the oscillations of the external current and thus the coherent state is less robust. As mentioned before, the FGSS in the $\kappa = \infty$ limit were explained in terms of a coherent oscillation of the vortex lattices formed when $I^e = 0$ [1,2,4]. When screening is included the ground-state vortex lattice configurations get modified. In the top left-hand frame of Fig. 3 we show an instantaneous vortex lattice configuration for the $\frac{1}{2}$ step in the $f = \frac{1}{2}$ case, with $\kappa = 2.27$, which oscillates with period two. We notice that there are "cluster" checkerboard regions, with structures as in the $\kappa = \infty$ case, separated by "Bloch" or "soliton" surface walls due to the screening currents. The size of the "cluster" regions in this particular case is about $l = 7a$ while the Bloch wall is $2a$. As $\kappa \to \kappa_c$, with $\kappa_c \leq 1$ the number of size $2a$ Bloch walls increases, and for $\kappa < \kappa_c$ the state is made of rows of constant vorticity (shown in the bottom left-hand frame in Fig. 3), a structure reminiscent of the intermediate state, although this one is dynamically generated. As is seen in Fig. 2(a) the $\kappa_c(f) \sim 1$. In the type-I regime the $I^e = 0$ field distributions correspond to the Meissner state. Starting from this state and turning on the external $I^e(t)$ current, the Lorentz force induced by $I^e(t)$ "pulls" the flux into the sample and, after a transient, the vortex distributions look as shown in the bottom left-hand frame of Fig. 3. The $\frac{1}{2}$ step in the IV characteristic corresponds to a coherent oscillation of the striped vortex distributions that oscillate between $+1$ and 0 vorticities with period two.

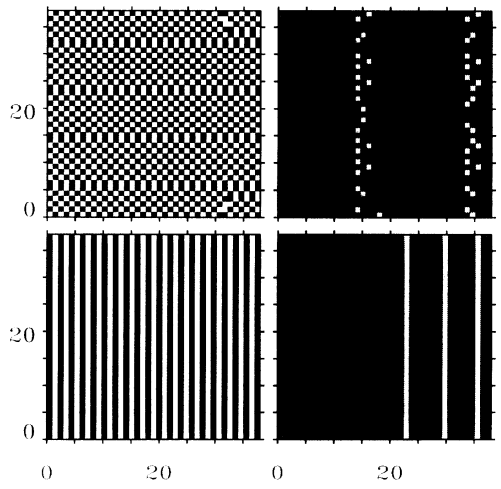

FIG. 3. Instantaneous vortex configurations for $\frac{1}{2}$ steps. Top left-hand frame corresponds to $f = \frac{1}{2}$ and $\kappa = 2.27$ (type II). Bottom left-hand frame corresponds to $f = \frac{1}{2}$ and $\kappa = 0.44$ (type I). White and black squares indicate 0 and $+1$ phase vorticity per plaquette, respectively. The phase vorticity is defined as $(1/2\pi)\sum\theta(\mathbf{r}) = \pm 1$. Right-hand frames correspond to $f = 0$ with $\kappa = 2.27$ (top) and $\kappa = 0.29$ (bottom). Same d as in 2(b). Here white, gray, and black indicate -1, 0, and $+1$ phase vorticity per plaquette, respectively.

We now move to consider the case when edge fields are explicitly included. First we show in Fig. 1(c) that for the case $f=\frac{1}{3}$ the step structure in the IV characteristics is qualitatively the same as in the $M=0$ case. The situation is different in the $f=0$ case, since for all the values of κ studied here there are half-integer GSS *only when* $M\neq 0$. In Fig. 2(b) we show the change in the $\frac{1}{2}$ step width ($f=0$) as a function of $1/\kappa$. First we note that, for $\kappa=\infty$, when we include the edge fields as boundary conditions, i.e., fixing $B_{\text{edge}}=\pm 1$ at the edges, we find that after a complicated transient the system settles exactly into the ACVS, including the angle of 27°, as discussed in Ref. [6], even when there are no defects in the sample. This result ($\kappa=\infty$) is marked as ACVS in Fig. 2(b). For finite κ, and free end boundary conditions, the edge fields are generated dynamically and the $\frac{1}{2}$ step width changes in a qualitatively similar way as when $f\neq 0$. Quantitatively the width of the $\frac{1}{2}$ step for $f=0$ is smaller than the $\frac{1}{2}$ step with $f=\frac{1}{2}$, and $\kappa_c(f=0)<\kappa_c(f)$. The microscopic vortex dynamics in both cases is very different. In the type-II regime ($f=0$) with $\kappa=2.27$, the oscillating vortex configurations consist of columns of *isolated* unit charged positive and negative vortices with period two. This state is shown in the top right-hand frame in Fig. 3. We see that as κ decreases from $\kappa=\infty$ to $1<\kappa\ll\infty$ the angle for the symmetry axis for vortex oscillations changes until it becomes collinear with the external current direction. The vortices are generated by the edge fields at the edges of the lattice. In the $\kappa<1$ limit we have two distinct vortex oscillatory motions with period two depending on whether $v<v_\Phi$ or $v>v_\Phi$. In the former case the vortex columns generated at the edges move towards the center of the array and collide, creating and annihilating individual vortices. In the regime where $v>v_\Phi$, the induced currents cannot follow the external one and thus the vortex stripes originating at the edges of the lattice do not have time to collide with each other while still oscillating back and forth with period two. This situation is shown in the bottom right-hand frame of Fig. 3. The experimental κ values are calculated in [1(b)] using Pearl's formula, which is valid in a continuous film. The value of $\kappa(T_c=3.5\text{ K})=280$ quoted in [1(b)] is in the type-II regime but with a $\lambda_L<N=1000$. For $T=2.5$ K a $\frac{1}{2}$ step was observed with a value for κ of 2.5, which is quite far from the extreme type-II regime. From our analysis we conclude that the $\frac{1}{2}$ step seen in [1(b)] is due to screening effects. The κ values considered here would then appear to correspond to their temperature range of [1.5 K, 2.5 K]. Also, the κ values in the experiments by Lee *et al.* [3(b)] correlate closely with our values. Furthermore, our discussion of the $\frac{1}{2}$ steps for $f=0$ gives support to the experimental finding in Nb-Au-Nb samples that edge fields are of importance in producing these steps [3(b)]. A further test of this assertion is provided by the inset in Fig. 2(b) that gives the $\frac{1}{2}$ step width as a function of f. This result is in good agreement with the corresponding result presented in Ref. [3(b)]. Although the results presented above correspond to $T=0$ we have verified that they are stable at low temperatures.

In conclusion, we have presented results of a study of the response of current driven Josephson-junction arrays including self-induced magnetic-field effects. A detailed analysis of the evolution of the vortex dynamics when going from type-II to type-I behavior was presented. We have found fractional giant Shapiro steps even in the extreme type-I regime, where self-field effects are dominant, and when the zero current ground state is the Meissner state. We have shown that giant fractional steps in the IV characteristics can be generated under many different circumstances, but for which the underlying microscopic vortex dynamics can be fundamentally different. Our results suggest that it would be very interesting if the real-time magnetic-field dynamics could be followed experimentally as done recently in experiments in high-T_c superconductors [11]. A detailed discussion of these and other related results will be presented elsewhere [10].

We thank J. Castro, A. Karma, and R. Markiewicz for useful discussions. We acknowledge NSF Grant No. DMR-9211339, the Pittsburgh Supercomputing Center Grant No. PHY88081P, and the Donors of the Petroleum Research Fund, Grant No. ACS-PRF#22036-AC6 for partial support of this research. D.D. was also supported by a fellowship from CONICET, Argentina.

[a]Permanent address: Centro Atómico Bariloche, 8400 San Carlos de Bariloche, Rio Negro, Argentina.

[1] (a) S. P. Benz *et al.*, Phys. Rev. Lett. **64**, 693 (1990); (b) S. P. Benz, Ph.D. thesis, Harvard University, 1990 (unpublished).

[2] L. L. Sohn *et al.*, Phys. Rev. B **45**, 3003 (1992); **44**, 925 (1991).

[3] (a) H. C. Lee *et al.*, Physica (Amsterdam) **165&166B**, 1571 (1990); (b) Phys. Rev. B **44**, 921 (1991); (c) S. H. Hebboul and J. Garland, *ibid.* **43**, 13703 (1991).

[4] K. H. Lee *et al.*, Phys. Rev. Lett. **64**, 962 (1990); K. H. Lee and D. Stroud, Phys. Rev. B **43**, 5280 (1991); J. U. Free *et al.*, Phys. Rev. B **41**, 7267 (1990); M. Octavio *et al.*, *ibid.* **44**, 4601 (1991); T. Halsey, *ibid.* **41**, 11634 (1990); M. Kvale and S. E. Hebboul, *ibid.* **43**, 3720 (1991); M. S. Rzchowski *et al.*, *ibid.* **43**, 8682 (1991).

[5] H. Eikmans and J. E. van Himbergen, Phys. Rev. B **44**, 6937 (1991); *ibid.* **41**, 8927 (1990).

[6] D. Domínguez *et al.*, Phys. Rev. Lett. **67**, 2367 (1991).

[7] W. Press *et al.*, *Numerical Recipes* (Cambridge Univ. Press, Cambridge, 1986).

[8] A. A. Abrikosov *et al.*, *Quantum Field Theoretical Methods in Statistical Physics* (Pergamon, New York, 1965), 2nd ed., p. 253.

[9] A. Majhofer *et al.*, Phys. Rev. B **44**, 9634 (1991).

[10] D. Domínguez and J. V. José (to be published).

[11] C. Durán *et al.*, Bull. Am. Phys. Soc. **37**, 538 (1992).

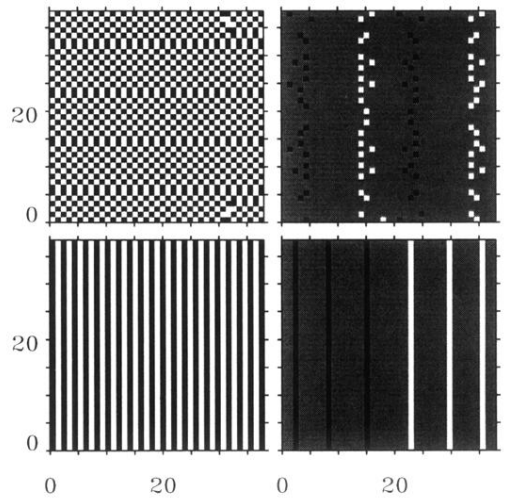

FIG. 3. Instantaneous vortex configurations for $\frac{1}{2}$ steps. Top left-hand frame corresponds to $f=\frac{1}{2}$ and $\kappa=2.27$ (type II). Bottom left-hand frame corresponds to $f=\frac{1}{2}$ and $\kappa=0.44$ (type I). White and black squares indicate 0 and $+1$ phase vorticity per plaquette, respectively. The phase vorticity is defined as $(1/2\pi)\sum\theta(\mathbf{r})=\pm 1$. Right-hand frames correspond to $f=0$ with $\kappa=2.27$ (top) and $\kappa=0.29$ (bottom). Same d as in 2(b). Here white, gray, and black indicate -1, 0, and $+1$ phase vorticity per plaquette, respectively.